In Situ Detection of Chemical Compositions at Nanodroplet Surfaces and In-Nanodroplet Phases

Journal:	*The Journal of Physical Chemistry*
Manuscript ID	jp-2022-03346s.R1
Manuscript Type:	Article
Date Submitted by the Author:	23-May-2022
Complete List of Authors:	Qian, Yuqin; Utah State University Brown, Jesse; Utah State University Zhang, Tong; Chinese Academy of Sciences, Institute of Chemistry Huangfu, Zhichao; Utah State University Rao, Yi; Utah State University College of Science, chemistry and biochemistry

In Situ Detection of Chemical Compositions at Nanodroplet Surfaces and In-Nanodroplet Phases

Yuqin Qian[#], Jesse B. Brown[#], Tong Zhang, Zhi-Chao Huang-Fu, and Yi Rao*

Department of Chemistry and Biochemistry, Utah State University, Logan, UT 84322, United States

Abstract

Small-volume nanodroplets play an increasingly common role in chemistry and biology. Such nanodroplets are believed to have unique chemical and physical properties at the interface between a droplet and its surrounding medium, however, they are underexamined. In this study, we present the novel technique of vibrational sum frequency scattering (VSFS) spectroscopy as an interface-specific, high-performance method for the *in situ* investigation of nanodroplets with sub-micron radii; as well as the droplet bulk through simultaneous hyper-Raman scattering (HRS) spectroscopy. We use laboratory-generated nanodroplets from aqueous alcohol solutions to demonstrate this technique's ability to separate the vibrational phenomena which take place at droplet surfaces from the underlying bulk phase. In addition, we systemically examine interfacial spectra of nanodroplets containing methanol, ethanol, 1-propanol, and 1-butanol through VSFS. Furthermore, we demonstrate interfacial differences between such nanodroplets and their analogous planar surfaces. The sensitivity of this technique to probe droplet surfaces with few-particle density at standard conditions validates VSFS as an analytical technique for the *in situ* investigation of small nanodroplets, providing breakthrough information about these species of ever-increasing relevance.

[#]Those authors contributed equally to this work.

***Corresponding Author:** E-mail (Yi Rao): yi.rao@usu.edu

Introduction

Small-volume nanodroplets (<1 pL) play an increasingly common role in chemistry and biology, from the streamlining and miniaturization of analyses and syntheses to the modeling of cells and atmospheric chemistry.[1-4] On a larger and more biologically focused scale, such nanodroplets hold great potential in intracellular treatment and manipulation.[5-6] Nanodroplets have also been employed in assaying samples with as few as tens of cells.[7] Similarly, the shift toward miniaturized analyses using sub-picoliter nanodroplets has invited groups to develop innovative methods of facilitating and improving these processes. [8-9] Although nanodroplets are already being employed in various applications, there is still much to be learned about the fundamental nature of such species. It has been thoroughly observed that chemical reactions in and on nanodroplets proceed at rates which are several orders of magnitude greater than in bulk solution.[4] To this effect, nanodroplets may reveal new avenues for efficient, on-demand chemical synthesis and production.[2, 10-11] A common method for investigating droplet reaction rate acceleration has been though electrospray ionization mass spectroscopy (ESI-MS), where charged nanodroplets are dispersed into the air where they can interact with each other and gas-phase species.[4, 12] Variations of MS have also been used to study systems of atmospheric and environmentally relevant nanodroplets. [13-16] While much information about reaction products and intermediates has been gained through these studies, not all bulk-phase reactions are accelerated in droplet species produced through this method, and ESI as a method for droplet dispersion should be cautioned.[17-18] Even so, a consistent conclusion can be drawn from these studies: the interface between nanodroplets and their surrounding medium plays a fundamental role in producing the unique properties of such species.

The outer monolayer of a droplet in contact with the surrounding media exhibits physical and chemical properties which are distinct from those of the underlying bulk. For nanodroplets of aqueous or soft matter origin, properties such as viscosity and partitioning rates mitigate overall chemical mobility upon the surface and within the droplet, directly affecting its properties of pH, uptake rates, and charge distribution.[19-21] Many such nanodroplets have a charged surface due to an increased ionic activity therein, giving rise to increased rates of solute activity and adsorption.[22-24] For these reasons, interface-specific forms of instrumental analysis are necessary to understand the orientation, kinetics, and structure dynamics at droplet interfaces.

The interfacial specificity of planar vibrational sum frequency generation (VSFG) spectroscopy has long been utilized to explore phase-partitioned interfaces,[25-28] more recently the interfacial interactions of more complex environmental, biological, and electrochemical systems.[23, 29-33] Producing pertinent environmental implications, VSFG experiments involving fatty acid coated aqueous interfaces have shown anions from dissolved salts can enhance deprotonation of interfacial fatty acids and provide qualitative improvements to VSFG signals without significantly affecting rates of interfacial ozonolysis, while also demonstrating that volatile products escape the fatty acid interface while less volatile species are reabsorbed into the system.[23, 34] VSFG has recently been catalogued as an analytical tool for

investigating the interfacial vibrations of various functional groups of proteins at biologically relevant interfaces, such as thin films, membranes, and synthetic substrates.[31] Some contemporary technological employments of VSFG utilize its interfacial specificity to characterize thin films of novel molecules in solar cells and to investigate fundamental interfacial phenomena in electrochemical systems.[32-33] While these studies and many more support the role of VSFG as a modern analytical technique for investigating vibrational phenomena at planar, phase-partitioned interfaces, these findings may not withstand the geometrical shift to droplet interfaces.

Recent previous efforts of our group into interfacial studies through nonlinear optical techniques have focused on development and optimization of second harmonic scattering (SHS) spectroscopy and demonstrating its capacity for measurement of the droplet surfaces and aqueous bulk simultaneously.[35] We have also demonstrated the validity of SHS as an analytical technique for the in situ analysis of the surface of nanodroplets using SHS-active dyes to show the effects of solvent polarity, salt concentration, and relative humidity on interfacial properties for such species.[36-37] We have recently been successful in quantitatively assessing the adsorption free energy, polarity, and molecular orientation of malachite green onto droplet surfaces through the development of electronic sum frequency scattering (ESFS), giving a direct view of the electronic properties of this interface.[38] In the current work, we present *in situ* vibrational sum frequency scattering (VSFS) spectroscopy from droplet surfaces alongside simultaneous hyper-Raman scattering (HRS) spectroscopy from the droplet as a whole. We compare the VSFS and HRS spectra of ethanol in nanodroplets, and present polarization-resolved VSFS spectra for methanol, ethanol, 1-propanol, and 1-butanol in aqueous nanodroplets. Finally, we demonstrate interfacial differences between the droplet surface and its planar analogue by contrasting VSFS and VSFG experiments.

Methods

Laser Sources. The laser source for droplet VSFS experiments was a 100.0 μJ, 290 fs pulse with a repetition rate of 100 kHz, and central wavelength of ca. 1026 nm (Pharos, Light Conversion). This system was used to pump an optical parametric amplifier (OPA) (ORHEUS-ONE, Light Conversion), generating a tunable IR beam from 2500 to 4500 nm. After selecting an IR beam with 3400 nm wavelength, the IR beam and residual 1026 nm exited the OPA were directed toward samples.

Optical Pathways. The 1026 nm pulse was directed first through a translational stage to manipulate temporal overlap, then passed through an air-spaced etalon (SLS Optics) to convert from the femtosecond pulse to a picosecond pulse, allowing spectral resolution of 8 cm^{-1}. Finally, a lens (f = 25 cm) focused the picosecond pulse onto the stream of nanodroplets with a diameter of about 90 μm. The IR beam with a typical pulse energy of 2.00 μJ underwent a similar manipulation by passing through a CaF_2 focusing lens with (f = 10 cm), producing an 80 μm beam diameter at the sample. The 1026 nm and IR beams were non-colinearly incident on the generated nanodroplets at 0° and 5° relative to the

X-axis, respectively. The 1026 nm and IR pulses form an incident plane parallel to the optical table and the XY-plane, as presented in Figure 1(A). The polarizations for each of the incident lights were independently controlled using half-wave plates.

Both the HRS bulk and VSFS signals were collected by 2" lenses, L3 and L5, (f = 2.5 cm) oriented at 0° and 90° relative to the forward propagating direction, respectively. Both signal collection setups utilized thin-film polarizers to select the desired signal polarization, 950 nm-short pass and 650 nm long-pass filters, and 2" lenses, L4 and L6, which focused the generated signals onto the slits of their respective spectrometers. Additionally, polarization of incident and signal radiation is defined relative to the optical table: H-polarization denotes horizontal orientation which is parallel to the bench, and V-polarization denotes a vertical orientation that is perpendicular to the bench.

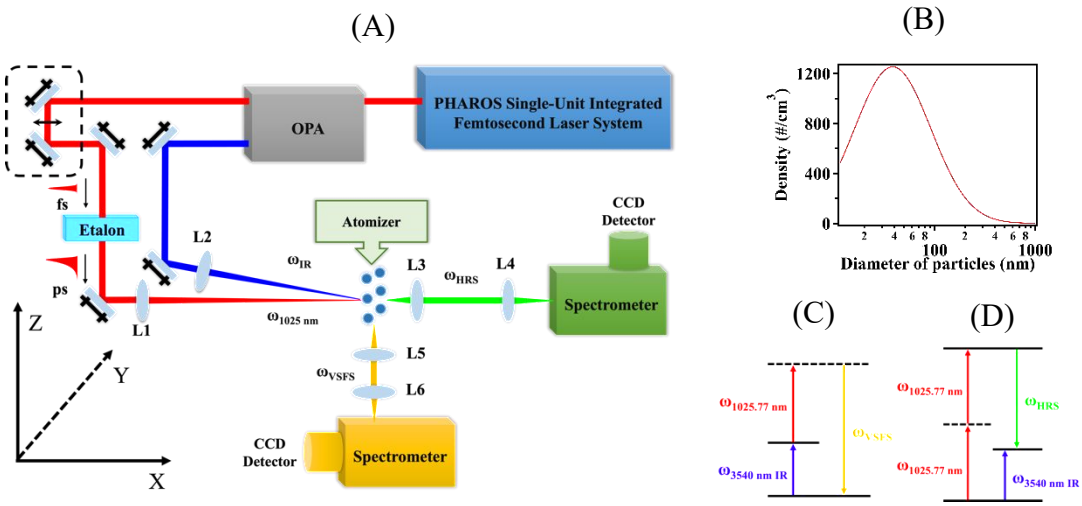

Figure 1: A) Schematic setup for simultaneous detection of interfacial VSFS and bulk HRS experiments. The optical table defines the XY-plane and nanodroplets flow along the Z-axis. B) Nanodroplet size distribution. C) Energy-level diagram for VSFS: $\omega_{VSFS} = \omega_{1026} + \omega_{IR}$, D) Energy-level diagram for HRS-bulk: $\omega_{HRS} = 2\omega_{1026} - \omega_{IR}$.

Spectral Collection. VSFS and HRS bulk spectra were detected through separate spectrometers (Acton 300i, Princeton Instruments) fitted with charge coupled device (CCD) detectors (Princeton Instruments, LN/CCD-1340/400). The short- and long-pass filters mentioned earlier in conjunction with the spectrometer provided blocking of remaining incident light and mitigation of darkroom background noise. Spectra from the CCD detectors were collected using WinSpec software (Princeton Instruments) with 300 s integration time and 30 s integration time per spectrum for both interfacial and bulk droplet species, respectively.

Droplet Generation. Nanodroplets were generated in the laboratory through a continuous flow atomizer (TSI 3076) fitted to a constant pressure of N_2 at 40 psi, and which drew from an aqueous stock solution of 0.5 M NaCl. A mass flow controller (MKS) was used to maintain continuous throughput of dispersed solution was held at 4 L/min, which resulted in a total density of approximately 3.8 × 10^6

nanodroplets/cm^3. For 0.5 M NaCl seed solution, the centered droplet size is about 40 nm, with its distribution from 10 to 300 nm.[35, 37-39] Generated nanodroplets were confined within a sealed chamber mounted on the optical bench with dimensions of 40 cm L × 30 cm W × 30 cm H. The chamber was equipped with an inlet for the droplet feed in the top panel, optical filters in side panels for incident and signal beams; and a catch-tube connected to a vacuum pump beneath the droplet output nozzle to ensure adequate ventilation.

Chemicals. 0.5 M NaCl seed solution was prepared in 18 MΩ.cm pure water with NaCl salt (Fisher Chemical), which had been dried at 600 °C for 10 hours. Methanol, (HPLC-UV grade, Pharmco), ethanol (200 proof, Pharmco), 1-propanol (Sigma-Aldrich, >99.5%), and 1-butanol (Mallinckrodt, 99.9%) were used as received to prepare experimental concentrations.

Finally, VSFG experiments of the planar air/liquid interface were conducted for ethanol mixtures in 0.5 M NaCl. This experimental setup has been described in detail elsewhere.[40]

Results & Discussion

Small-volume nanodroplets have unique properties regarding their surface and bulk compositions. For this reason, our VSFS technique is well-suited to analyze such species, allowing for the simultaneous observation of the vibrational characteristics of the droplet surface and bulk phase directly. As a second-order nonlinear process, sum frequency responses are forbidden from systems exhibiting centrosymmetry. For this reason, VSFS has been chosen to specifically probe the surface of nanodroplets where molecular centrosymmetry is broken. On the other hand, the hyper-Raman technique is a third-order nonlinear process and therefore possesses no surface specificity. Hence, we have chosen HRS as a probe to investigate the vibrational properties of nanodroplets as a whole. Precise spatial and tuned temporal overlap of ω_{1026} and ω_{IR} incident pulses upon a steam of nanodroplets gives a VSFS signal at $\omega_{SFS} = \omega_{1026} + \omega_{IR}$ (Figure 1C) and a signal form the droplet bulk which has tentatively been labeled as HRS at $\omega_{HRS} = 2\omega_{1026} - \omega_{IR}$ (Figure 1D).

Figure 2A shows emission spectra of nanodroplets generated from the same solution of 10 M ethanol in aqueous 0.5 M NaCl. The VSFS spectrum (upper) was collected by observing the generated signal centered at 787 nm, giving three distinct peaks. These peaks, at 2879.7, 2932.8, and 2981.3 cm^{-1}, have been assigned according to the conventions for VSFG of a planar interface as the $-CH_3^{(ss)}$/$-CH_2^{(ss)}$, $-CH_3$ Fermi resonance, and $-CH_3^{(as)}$/$-CH_2$ Fermi resonance, respectively.[41-42] The corresponding HRS bulk spectrum (lower) of the same sample was collected by observing a central wavelength of 605 nm. This spectrum contains a peak at 2887.9 cm^{-1} for $-CH_3^{(ss)}$, a shoulder near 2930.1 cm^{-1} for the $-CH_3$

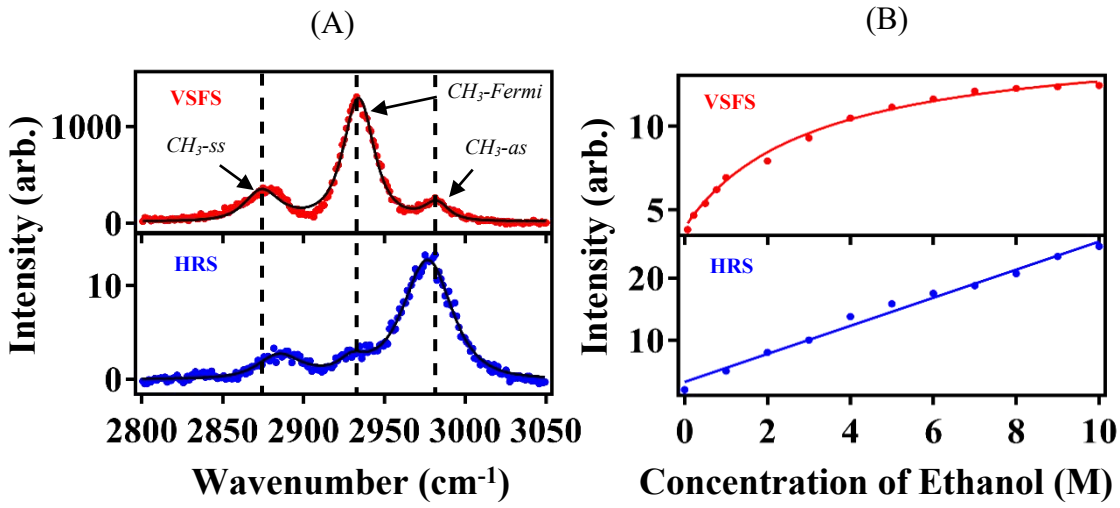

Figure 2: A) VSFS (top) and HRS (bottom) spectra of nanodroplets from 10 M ethanol in 0.5 M NaCl seed solution. Both spectra are in HHH polarization configurations. B) Signal intensity versus ethanol concentration in stock solution for VSFS (top), $-CH_3$ Fermi at 2932.8 cm^{-1}; and HRS (bottom), $-CH_3$ Fermi at 2930.1 cm^{-1}.

Fermi resonance, and a peak at 2977.7 cm^{-1} that represents $-CH_3^{(as)}$.[43-44] While the peaks for VSFS and HRS spectra are nearly in line with each other for the corresponding vibrational modes, there is a discrepancy in relative peak intensities. For the VSFS spectrum, the intensity is greatest for the Fermi peak and decreases with the symmetric and asymmetric modes. Conversely, the HRS bulk spectrum gives the most intense response for the $-CH_3$ asymmetric mode, followed by the symmetric stretch; both of which nearly overshadow the Fermi resonance signal. These spectral differences may arise from molecular orientations being more ordered at the droplet surface compared to a random orientation in the bulk.

To further identify surface and bulk behaviors, VSFS and HRS spectra were collected from laboratory-generated nanodroplets with increasing ethanol concentrations from 0 to 10 M in 0.5 M NaCl aqueous stock solution. These concentration dependent VSFS and HRS $-CH_3$ Fermi intensities are shown in Figure 2B. While the VSFS electric field follows a Langmuir-type distribution with increasing concentration,[45] HRS intensity increases linearly as expected.[46] Concentration isotherms for all HRS peaks can be found in the Supporting Information. This further demonstrates that the VSFS spectra are,

in fact, of interface origin, representing the partitioning of ethanol molecules to the droplet surface with increasing bulk concentration.

An increased understanding of molecular structure and orientation can reveal the understudied nature of chemical reactions at droplet surfaces. Polarization-resolved interfacial vibrational spectra can give a detailed description of the structure and molecular orientation at an interface as each polarization combination yields a unique spectrum.[26, 47] In Figure 3, the VSFS spectra of nanodroplets from a stock solution of 10 M ethanol are shown for HHH, HVV, VHV, and VVH. The HHH polarization gives a spectrum with peaks prescribed above and VVH polarization shows the -$CH_3^{(ss)}$ at 2879.7cm^{-1} and the -CH_3 Fermi resonance at 2937.9 cm^{-1} which is shifted about 4 cm^{-1} relative to the HHH spectrum. Although the VHV spectrum shows no discernable peaks, the HVV spectrum contains a comparatively slight -$CH_3^{(as)}$ peak at 2973 cm^{-1}.

For the planar air/liquid interface, polarized VSFG has been proven as an analytical technique for quantitatively uncovering interfacial molecular orientations.[48-49] Correspondingly, a method for calculating interfacial molecular orientation at the surface of nanodroplets using VSFS has been developed.[50] While this theory has a very strong basis, it does not align with our experimental results. Based on the current VSFS theory, spectral intensities for the VVH polarization should exceed those of the HHH polarization for both -$CH_3^{(ss)}$ and -$CH_3^{(as)}$ modes, however, our results show the opposite case. It was suggested that local field factors might should be taken into account. The nonlinear Mie scattering theory fails in our case since the refractive indexes of air and water are significantly different. Thus, the susceptibilities from the measured polarization combinations, $\chi^{(2)}_{LMN}$ (*L,M,N: V* or *H*), are related to susceptibilities local laboratory coordinate (X,Y,Z), $\chi^{(2)}_{IJK}$ (*I,J,K: X, Y, Z*), as follows:[26, 51]

$$\chi^{(2)}_{VVH} = L_{yy}(\omega)L_{yy}(\omega_1)L_{zz}(\omega_2)\sin\beta_2\chi^{(2)}_{YYZ}$$
$$\chi^{(2)}_{VHV} = L_{yy}(\omega)L_{zz}(\omega_1)L_{yy}(\omega_2)\sin\beta_1\chi^{(2)}_{YZY}$$
$$\chi^{(2)}_{HVV} = L_{zz}(\omega)L_{yy}(\omega_1)L_{yy}(\omega_2)\sin\beta\chi^{(2)}_{ZYY}$$
$$\begin{aligned}\chi^{(2)}_{HHH} = &-L_{xx}(\omega)L_{xx}(\omega_1)L_{zz}(\omega_2)\cos\beta\cos\beta_1\sin\beta_2\chi^{(2)}_{XXZ}\\ &-L_{xx}(\omega)L_{zz}(\omega_1)L_{xx}(\omega_2)\cos\beta\sin\beta_1\cos\beta_2\chi^{(2)}_{XZX}\\ &+L_{zz}(\omega)L_{xx}(\omega_1)L_{xx}(\omega_2)\sin\beta\cos\beta_1\cos\beta_2\chi^{(2)}_{ZXX}\\ &+L_{zz}(\omega)L_{zz}(\omega_1)L_{zz}(\omega_2)\sin\beta\sin\beta_1\sin\beta_2\chi^{(2)}_{ZZZ}\end{aligned} \quad (1)$$

where $L_{ii}(\omega)$ (*ii*: *xx, yy*, and *zz*) denotes local field factors, which has to be fully taken into account in our case. Nevertheless, the polarized VSFS spectra in Figure 3 may still provide some qualitative interfacial orientation information. If the orientation of the ethanol methyl group was distributed randomly across the nanodroplet's surface, all four polarization configurations should produce similar spectra. Since HHH and VVH polarizations provide the richest spectra for our experiments while HVV and VHV barely show any signal, it can be inferred that the methyl group behaves in an ordered manner at the nanodroplet surface.

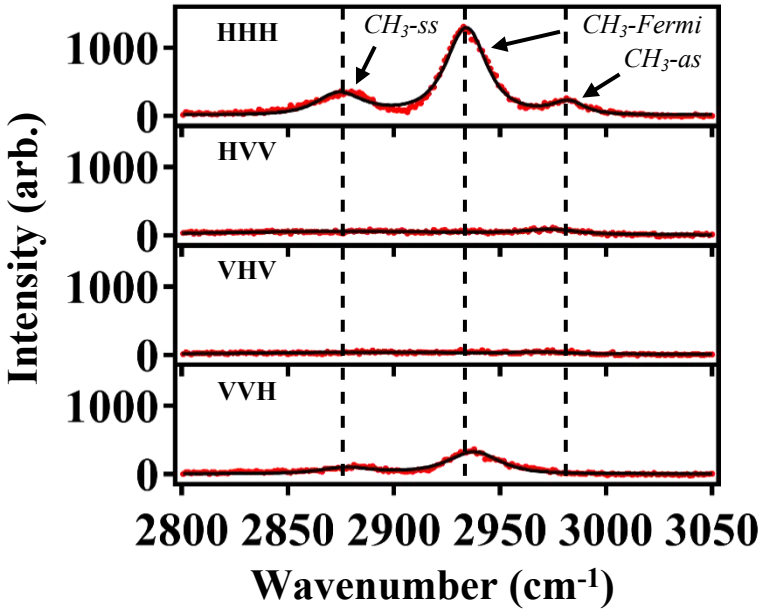

Figure 3. VSFS spectra of nanodroplets generated from 10 M ethanol in 0.5 M NaCl seed solution measured at different polarization combinations: HHH, HVV, VHV, and VVH.

Vibrational sum frequency generation scattering is anticipated to be an analytical technique for the characterization of interfacial molecular species.[50, 52-54] To assess our *in situ* VSFS technique, we have

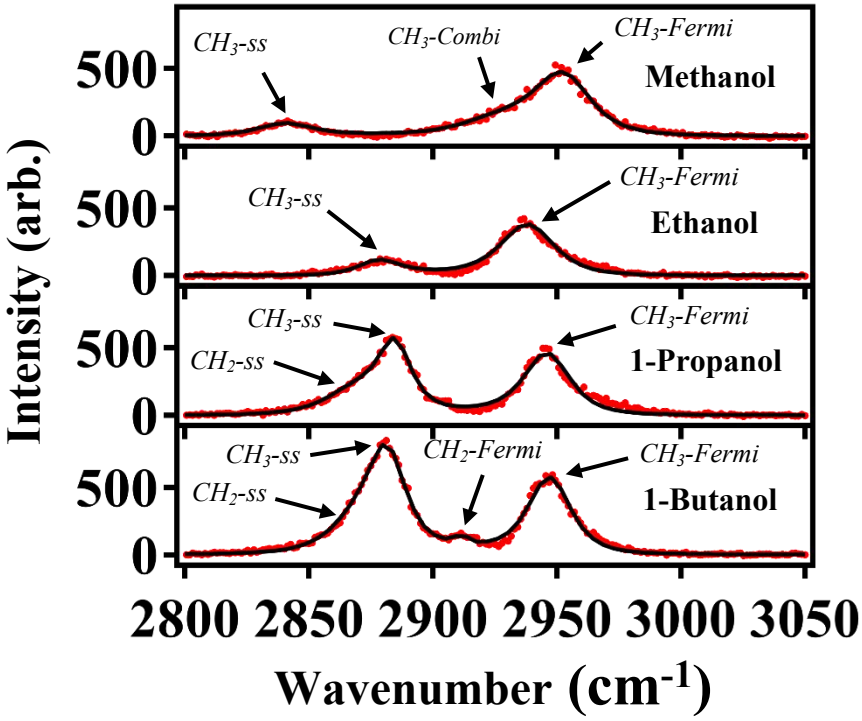

Figure 4. VVH-polarized spectra of droplet surfaces for methanol, ethanol, propanol, and butanol. All alcohol concentrations were taken at 10 M in 0.5 M NaCl stock solution.

collected polarized VSFS spectra from droplet surfaces for solutions of methanol, ethanol, 1-propanol, and 1-butanol solutions in 0.5 M NaCl. These normalized spectra collected at VVH polarization are shown in Figure 4; corresponding spectra at other polarizations can be found the Supporting Information along with all fitting parameters. Beginning with the smallest of the alcohols, the VSFS spectrum of methanol nanodroplets contains two distinct peaks at 2841.4 and 2951.9 cm^{-1} which correspond to the $-CH_3^{(ss)}$ and $-CH_3$ Fermi modes, respectively. VSFS spectra for 1-propanol and -butanol in Figures 4 are prescribed with the following vibrational modes: prominent $-CH_3^{(ss)}$ at 2881.2 cm^{-1}, comparatively weak $-CH_2$ Fermi resonance at 2908.8 cm^{-1}, and the $-CH_3$ Fermi resonance at 2945.5 cm^{-1}.[38] These spectral peaks for the alcohols are consistent with those reported in the literature.[42] It is interesting to note that our VSFS spectra of nanodroplets have red spectral shift of about 10 cm^{-1} relative to the planar surface.[42] Methanol exhibits a significant blue shift in its $-CH_3^{(ss)}$ mode, relative to that of the other alcohols, and is the only one of the four species which also displays a $-CH_3^{(as)}$ peak. On the surface of nanodroplets, ethanol only exhibits the $-CH_3^{(ss)}$ and $-CH_3$ Fermi peaks, the latter is slightly blue-shifted relative to that of the longer-chain alcohols. Finally, 1-propanol and 1-butanol are characterized by the three $-CH_3^{(ss)}$, $-CH_2$ Fermi, and $-CH_3$ Fermi peaks, with the intensity of the $-CH_2$ Fermi resonance mode distinguishing the two. These results enabled us to characterize functional groups at the surface of nanodroplets.

Not only do droplet surfaces exhibit chemical and physical properties which are distinct from the corresponding bulk solution, these features may not be readily analogous to the planar air/liquid interface. Sum frequency intensity is proportional to the surface number density.[26, 50, 55] Therefore, we have compared the concentration isotherms for ethanol at droplet and air/liquid interfaces. Concentration isotherms of ethanol in 0.5 M NaCl, with VSFS in red and VSFG in blue, are shown in Figure 5. The intensity of the $-CH_3^{(ss)}$ resonance quickly reaches a maximum for the VSFG experiment at a concentration of 1 M, then decreases with larger concentrations as expected.[48, 56] Once the surface number density of ethanol reaches a critical point, the sum frequency intensity starts to become cancelled out by the formation of a sub-surface monolayer which contains molecules oriented antiparallel to the interfacial molecules.

Modeling of solutes partitioning to liquid surfaces by the Langmuir isotherm is given by

$$\sqrt{I_{VSFS}} \propto E_{VSFS} \propto \frac{Ns}{N_\infty} \propto \frac{Kc}{Kc + 55.5} \tag{2}$$

Where I_{VSFS} is the VSFS signal intensity, N_S is the effective interfacial density, N_∞ is the interfacial density for a full first layer coverage, K is the adsorption equilibrium constants, and c is the bulk concentration of solute. The fittings of Eq. (2) to the two concentration isotherms of ethanol in Figure 5 yield K values of 21.04 ± 1.96 for nanodroplets and 517.2 ± 90.4 for the air/liquid surface. The adsorption free energies are on the order of -7.55 ± 0.01 kJ/mol and -15.49 ± 0.01 kJ/mol, respectively, providing a means to quantify the surface-affinity of an adsorbate for a given surface. On the other hand, ethanol molecules partition to the spherical droplet surface in a Langmuir-type trend. This discrepancy in interfacial partitioning rates may be caused by a large pressure gradient across the radius of the droplet produced by its highly curved surface.[57-59] Thus, the mobility of ethanol molecules in nanodroplets may be much lower than that of the planar analogue, resulting in a decreased interfacial partitioning rate. It is possible that this increased pressure along with the lessened availability of analyte molecules inhibits of a cancelling secondary monolayer. The mobility of dispersed species within and upon nanodroplets is crucial to understanding dynamics and reaction kinetics for such species as it controls the partitioning of reaction products throughout nanodroplets.

The demonstration herein of the unique nature of the droplet surface confirms that processes will occur differently at the droplet surface relative to the bulk solution. Using VSFS to observe vibrational phenomena at the surface of nanodroplets, and HRS scattering for the droplet bulk, will allow for the *in situ* monitoring of adsorptions and reactions as they progress across the droplet radius. This technique will provide valuable information to models, aiding in atmospheric and climate modeling. Finally, the ability of VSFS to characterize interfacial species at the highly curved surface of small nanodroplets can provide precise information of interactions at biological interfacial systems such as bioreactors and sensors; and to increase the fundamental knowledge of this unique system, strengthening the backbone of this broadening field of study.

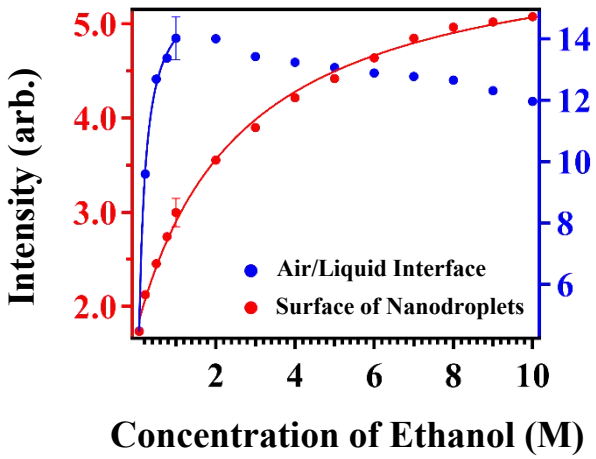

Figure 5. Concentration isotherm comparison of the surface of nanodroplets and the air/liquid interface for 0-10 M ethanol in 0.5 M NaCl, observing -$CH_3^{(as)}$ peak intensity for VSFS (surface of nanodroplets) and VSFG (air/liquid interface) at HHH polarizations.

Conclusions

We have demonstrated a technique which allows for the simultaneous observation of vibrational phenomena from both the droplet surface through VSFS as well as the droplet bulk through HRS scattering spectroscopies. The ability of this technique to monitor species at and beneath the surface of nanodroplets opens the door for studying processes which are dynamic as they proceed from the nanodroplet surface into the underlying bulk. Analysis of VSFS spectra of short-chained alcohols has shown that this technique can be a useful tool in characterizing species present at the surface of nanodroplets in air. Polarization-resolved VSFS spectra also demonstrated that molecular orientation is ordered at droplet surfaces, which can impact current models for atmospheric, biological, and synthetic processes. We have also shown that the affinity of ethanol molecules for surface activity is hindered at nanodroplet surfaces relative to the planar air/liquid interface, which is often considered negligible. Current efforts by our group are being devoted to uncovering and applying a VSFS theory to provide quantitative molecular orientations from our experiments. Further research is underway by our group to investigate the droplet size and viscosity dependence of interfacial partitioning, as well as reaction

and adsorption rates at droplet surfaces to elucidate the chemical and physical properties of such a unique and important system.

Notes

The authors declare no competing financial interests.

ACKNOWLEDGMENT

This material is based upon work supported by the National Science Foundation under Grant No. [2045084].

Supporting Information. Hyper-Raman Scattering (HRS) concentration isotherms; polarized vibrational sum frequency scattering (VSFS) spectra of methanol, 1-propanol, and 1-butanol; spectral fitting parameters for VSFS spectra.

References

1. Wang, W.; Yang, C.; Li, C. M., Efficient on-Demand Compound Droplet Formation: From Microfluidics to Microdroplets as Miniaturized Laboratories. *Small* **2009**, *5*, 1149-1152.
2. Dyett, B. P.; Zhang, X., Accelerated Formation of H2 Nanobubbles from a Surface Nanodroplet Reaction. *ACS Nano* **2020**, *14*, 10944-10953.
3. Kolb, C. E.; Worsnop, D. R., Chemistry and Composition of Atmospheric Aerosol Particles. *Annu. Rev. Phys. Chem.* **2012**, *63*, 471-91.
4. Wei, Z.; Li, Y.; Cooks, R. G.; Yan, X., Accelerated Reaction Kinetics in Microdroplets: Overview and Recent Developments. *Annu. Rev. Phys. Chem.* **2020**, *71*, 31-51.
5. Moyano, D. F.; Rotello, V. M., Nano Meets Biology: Structure and Function at the Nanoparticle Interface. *Langmuir* **2011**, *27*, 10376-10385.
6. Raj, D. B. T. G.; Khan, N. A., Designer Nanoparticle: Nanobiotechnology Tool for Cell Biology. *Nano Converg.* **2016**, *3*, 1-12.
7. Zhu, Y., et al., Nanodroplet Processing Platform for Deep and Quantitative Proteome Profiling of 10–100 Mammalian Cells. *Nat. Commun.* **2018**, *9*, 882.
8. Shan, C.; Zhang, C.; Liang, J.; Yang, Q.; Bian, H.; Yong, J.; Hou, X.; Chen, F., Femtosecond Laser Hybrid Fabrication of a 3d Microfluidic Chip for Pcr Application. *Opt. Express* **2020**, *28*, 25716-25722.
9. Kim, H.; Dixit, S.; Green, C. J.; Faris, G. W., Nanodroplet Real-Time Pcr System with Laser Assisted Heating. *Opt. Express* **2009**, *17*, 218-227.
10. Li, Z.; Kiyama, A.; Zeng, H.; Lohse, D.; Zhang, X., Speeding up Biphasic Reactions with Surface Nanodroplets. *Lab Chip* **2020**, *20*, 2965-2974.
11. Bain, R. M.; Sathyamoorthi, S.; Zare, R. N., "On-Droplet" Chemistry: The Cycloaddition of Diethyl Azodicarboxylate and Quadricyclane. *Angew. Chem. Int. Ed.* **2017**, *56*, 15083-15087.
12. Yan, X.; Bain, R. M.; Cooks, R. G., Organic Reactions in Microdroplets: Reaction Acceleration Revealed by Mass Spectrometry. *Angew. Chem. Int. Ed.* **2016**, *55*, 12960-12972.
13. Lim, C. Y.; Browne, E. C.; Sugrue, R. A.; Kroll, J. H., Rapid Heterogeneous Oxidation of Organic Coatings on Submicron Aerosols. *Geophys. Res. Lett.* **2017**, *44*, 2949-2957.

14. Arata, C.; Heine, N.; Wang, N.; Misztal, P. K.; Wargocki, P.; Beko, G.; Williams, J.; Nazaroff, W. W.; Wilson, K. R.; Goldstein, A. H., Heterogeneous Ozonolysis of Squalene: Gas-Phase Products Depend on Water Vapor Concentration. *Environ Sci Technol* **2019**, *53*, 14441-14448.

15. Chim, M. M.; Lim, C. Y.; Kroll, J. H.; Chan, M. N., Evolution in the Reactivity of Citric Acid toward Heterogeneous Oxidation by Gas-Phase Oh Radicals. *ACS Earth Space Chem.* **2018**, *2*, 1323-1329.

16. Gu, A. Y.; Musgrave, C.; Goddard, W. A., 3rd; Hoffmann, M. R.; Colussi, A. J., Role of Ferryl Ion Intermediates in Fast Fenton Chemistry on Aqueous Microdroplets. *Environ Sci Technol* **2021**, *55*, 14370-14377.

17. Banerjee, S.; Gnanamani, E.; Yan, X.; Zare, R. N., Can All Bulk-Phase Reactions Be Accelerated in Microdroplets? *Analyst* **2017**, *142*, 1399-1402.

18. Rovelli, G.; Jacobs, M. I.; Willis, M. D.; Rapf, R. J.; Prophet, A. M.; Wilson, K. R., A Critical Analysis of Electrospray Techniques for the Determination of Accelerated Rates and Mechanisms of Chemical Reactions in Droplets. *Chem. Sci.* **2020**, *11*, 13026-13043.

19. Mai, H.; Shiraiwa, M.; Flagan, R. C.; Seinfeld, J. H., Under What Conditions Can Equilibrium Gas–Particle Partitioning Be Expected to Hold in the Atmosphere? *Environ. Sci. Technol.* **2015**, *49*, 11485-11491.

20. Nozière, B.; Baduel, C.; Jaffrezo, J.-L., The Dynamic Surface Tension of Atmospheric Aerosol Surfactants Reveals New Aspects of Cloud Activation. *Nat. Commun.* **2014**, *5*, 3335.

21. Kallay, N.; Preočanin, T.; Selmani, A.; Kovačević, D.; Lützenkirchen, J.; Nakahara, H.; Shibata, O., Thermodynamic Model of Charging the Gas/Water Interface. *J. Phys. Chem. C* **2015**, *119*, 997-1007.

22. Mishra, H.; Enami, S.; Nielsen, R. J.; Hoffmann, M. R.; Goddard, W. A., 3rd; Colussi, A. J., Anions Dramatically Enhance Proton Transfer through Aqueous Interfaces. *Proc. Natl. Acad. Sci. U.S.A.* **2012**, *109*, 10228-32.

23. Casillas-Ituarte, N. N.; Callahan, K. M.; Tang, C. Y.; Chen, X.; Roeselova, M.; Tobias, D. J.; Allen, H. C., Surface Organization of Aqueous Mgcl2 and Application to Atmospheric Marine Aerosol Chemistry. *Proc. Natl. Acad. Sci. U.S.A.* **2010**, *107*, 6616-21.

24. Jungwirth, P.; Tobias, D. J., Ions at the Air/Water Interface. *J. Phys. Chem. B* **2002**, *106*, 6361-6373.

25. Zhang, D.; Gutow, J.; Eisenthal, K.; Heinz, T., Sudden Structural Change at an Air/Binary Liquid Interface: Sum Frequency Study of the Air/Acetonitrile–Water Interface. *J. Chem. Phys.* **1993**, *98*, 5099-5101.

26. Wang, H.-F.; Gan, W.; Lu, R.; Rao, Y.; Wu, B.-H., Quantitative Spectral and Orientational Analysis in Surface Sum Frequency Generation Vibrational Spectroscopy (Sfg-Vs). *Int. Rev. Phys. Chem.* **2005**, *24*, 191-256.

27. Chen, Z.; Shen, Y. R.; Somorjai, G. A., Studies of Polymer Surfaces by Sum Frequency Generation Vibrational Spectroscopy. *Annu. Rev. Phys. Chem.* **2002**, *53*, 437-65.

28. Sung, J.; Park, K.; Kim, D., Surfaces of Alcohol−Water Mixtures Studied by Sum-Frequency Generation Vibrational Spectroscopy. *J. Phys. Chem. B* **2005**, *109*, 18507-18514.

29. Kleber, J.; Laß, K.; Friedrichs, G., Quantitative Time-Resolved Vibrational Sum Frequency Generation Spectroscopy as a Tool for Thin Film Kinetic Studies: New Insights into Oleic Acid Monolayer Oxidation. *J. Phys. Chem. A* **2013**, *117*, 7863-7875.

30. Ebben, C. J.; Ault, A. P.; Ruppel, M. J.; Ryder, O. S.; Bertram, T. H.; Grassian, V. H.; Prather, K. A.; Geiger, F. M., Size-Resolved Sea Spray Aerosol Particles Studied by Vibrational Sum Frequency Generation. *J. Phys. Chem. A* **2013**, *117*, 6589-6601.

31. Hosseinpour, S.; Roeters, S. J.; Bonn, M.; Peukert, W.; Woutersen, S.; Weidner, T., Structure and Dynamics of Interfacial Peptides and Proteins from Vibrational Sum-Frequency Generation Spectroscopy. *Chem. Rev.* **2020**, *120*, 3420-3465.
32. Magomedov, A.; Al-Ashouri, A.; Kasparavičius, E.; Strazdaite, S.; Niaura, G.; Jošt, M.; Malinauskas, T.; Albrecht, S.; Getautis, V., Self-Assembled Hole Transporting Monolayer for Highly Efficient Perovskite Solar Cells. *Adv. Energy Mater.* **2018**, *8*, 9.
33. Peng, Q.; Chen, J.; Ji, H.; Morita, A.; Ye, S., Origin of the Overpotential for the Oxygen Evolution Reaction on a Well-Defined Graphene Electrode Probed by in Situ Sum Frequency Generation Vibrational Spectroscopy. *J. Am. Chem. Soc.* **2018**, *140*, 15568-15571.
34. Voss, L. F.; Bazerbashi, M. F.; Beekman, C. P.; Hadad, C. M.; Allen, H. C., Oxidation of Oleic Acid at Air/Liquid Interfaces. *J. Geophys. Res.* **2007**, *112*.
35. Qian, Y.; Deng, G. H.; Rao, Y., In Situ Chemical Analysis of the Gas-Aerosol Particle Interface. *Anal. Chem.* **2018**, *90*, 10967-10973.
36. Fang, H.; Ma, J.; Wilhelm, M. J.; Rao, Y.; Kuhn, D. L.; Zander, Z.; DeLacy, B. G.; Dai, H.-L., Carboxylic Anchoring Dye P-Ethyl Red Does Not Adsorb Directly onto Tio2 Particles in Protic Solvents. *J. Phys. Chem. C* **2019**, *123*, 8265-8272.
37. Qian, Y.; Deng, G. H.; Lapp, J.; Rao, Y., Interfaces of Gas-Aerosol Particles: Relative Humidity and Salt Concentration Effects. *J Phys Chem A* **2019**, *123*, 6304-6312.
38. Qian, Y.; Deng, G. H.; Rao, Y., In Situ Spectroscopic Probing of Polarity and Molecular Configuration at Aerosol Particle Surfaces. *J Phys Chem Lett* **2020**, *11*, 6763-6771.
39. Wu, Y.; Li, W.; Xu, B.; Li, X.; Wang, H.; McNeill, V. F.; Rao, Y.; Dai, H. L., Observation of Organic Molecules at the Aerosol Surface. *J Phys Chem Lett* **2016**, *7*, 2294-7.
40. Deng, G. H.; Qian, Y.; Zhang, T.; Han, J.; Chen, H.; Rao, Y., Two-Dimensional Electronic-Vibrational Sum Frequency Spectroscopy for Interactions of Electronic and Nuclear Motions at Interfaces. *Proc. Natl. Acad. Sci. U.S.A.* **2021**, *118*.
41. Gan, W.; Zhang, Z.; Feng, R.-r.; Wang, H.-f., Identification of Overlapping Features in the Sum Frequency Generation Vibrational Spectra of Air/Ethanol Interface. *Chem. Phys. Lett.* **2006**, *423*, 261-265.
42. Lu, R.; Gan, W.; Wu, B.-h.; Zhang, Z.; Guo, Y.; Wang, H.-f., C−H Stretching Vibrations of Methyl, Methylene and Methine Groups at the Vapor/Alcohol (N = 1−8) Interfaces. *J. Phys. Chem. B* **2005**, *109*, 14118-14129.
43. Okuno, M., Hyper-Raman Spectroscopy of Alcohols Excited at 532 Nm: Methanol, Ethanol, 1-Propanol, and 2-Propanol. *J. Raman Spectrosc.* **2021**, *52*, 849-856.
44. Ault, A. P.; Zhao, D.; Ebben, C. J.; Tauber, M. J.; Geiger, F. M.; Prather, K. A.; Grassian, V. H., Raman Microspectroscopy and Vibrational Sum Frequency Generation Spectroscopy as Probes of the Bulk and Surface Compositions of Size-Resolved Sea Spray Aerosol Particles. *Phys. Chem. Chem. Phys.* **2013**, *15*, 6206-6214.
45. Van Assche, T. R. C.; Baron, G. V.; Denayer, J. F. M., An Explicit Multicomponent Adsorption Isotherm Model: Accounting for the Size-Effect for Components with Langmuir Adsorption Behavior. *Adsorption* **2018**, *24*, 517-530.
46. Ringholm, M.; Bast, R.; Oggioni, L.; Ekstrom, U.; Ruud, K., Analytic Calculations of Hyper-Raman Spectra from Density Functional Theory Hyperpolarizability Gradients. *J Chem Phys* **2014**, *141*, 134107.
47. Wang, H. F.; Velarde, L.; Gan, W.; Fu, L., Quantitative Sum-Frequency Generation Vibrational Spectroscopy of Molecular Surfaces and Interfaces: Lineshape, Polarization, and Orientation. *Annu. Rev. Phys. Chem.* **2015**, *66*, 189-216.

48. Hua Chen, W. G., Bao-hua Wu, Dan Wu, Yuan Guo, and Hong-fei Wang, Determination of Structure and Energetics for Gibbs Surface Adsorption Layers of Binary Liquid Mixture 1. Acetone + Water. *J. Phys. Chem. B.* **2005**, *109*, 8053-8063.
49. Chen, H.; Gan, W.; Wu, B.-h.; Wu, D.; Zhang, Z.; Wang, H.-f., Determination of the Two Methyl Group Orientations at Vapor/Acetone Interface with Polarization Null Angle Method in Sfg Vibrational Spectroscopy. *Chem. Phys. Lett.* **2005**, *408*, 284-289.
50. de Beer, A. G.; Roke, S., Obtaining Molecular Orientation from Second Harmonic and Sum Frequency Scattering Experiments in Water: Angular Distribution and Polarization Dependence. *J Chem Phys* **2010**, *132*, 234702.
51. de Beer, A. G. F., Roke, S., and Dadap, J. I., Theory of Second-Harmonic and Sum-Frequency Scattering from Arbitrarily Shaped Particles. *J. Opt. Soc. Am. B.* **2011**, *28*, 1374-1384.
52. Roke, S.; Roeterdink, W. G.; Wijnhoven, J. E. G. J.; Petukhov, A. V.; Kleyn, A. W.; Bonn, M., Vibrational Sum Frequency Scattering from a Submicron Suspension. *Phys. Rev. Lett.* **2003**, *91*, 258302.
53. Kulik, S.; Pullanchery, S.; Roke, S., Vibrational Sum Frequency Scattering in Absorptive Media: A Theoretical Case Study of Nano-Objects in Water. *J. Phys. Chem. C* **2020**, *124*, 23078-23085.
54. Foster, M. J.; Carpenter, A. P.; Richmond, G. L., Dynamic Duo: Vibrational Sum Frequency Scattering Investigation of Ph-Switchable Carboxylic Acid/Carboxylate Surfactants on Nanodroplet Surfaces. *J. Phys. Chem. B* **2021**, *125*, 9629-9640.
55. Heike Arnoldsa, M. B., ∗, Ultrafast Surface Vibrational Dynamics. *Surf. Sci. Rep.* **2010**, *65*, 45-66.
56. Chen, H.; Gan, W.; Lu, R.; Guo, Y.; Wang, H.-f., Determination of Structure and Energetics for Gibbs Surface Adsorption Layers of Binary Liquid Mixture 2. Methanol + Water. *J. Phys. Chem. B* **2005**, *109*, 8064-8075.
57. Riva, M., et al., High Pressure inside Nanometer-Sized Particles Influences the Rate and Products of Chemical Reactions. *Environ Sci Technol* **2021**, *55*, 7786-7793.
58. Nakajima, R.; Miura, A.; Abe, S.; Kitamura, N., Optical Trapping-Polarized Raman Microspectroscopy of Single Ethanol Aerosol Microdroplets: Droplet Size Effects on Rotational Relaxation Time and Viscosity. *Anal. Chem.* **2021**, *93*, 5218-5224.
59. Tsuji, K.; Müller, S. C., Chemical Reaction Evolving on a Droplet. *J. Phys. Chem. Lett.* **2012**, *3*, 977-980.

TOC Image